Measurements on Partially Coherent Light

J. Woudenberg

February 19, 2010

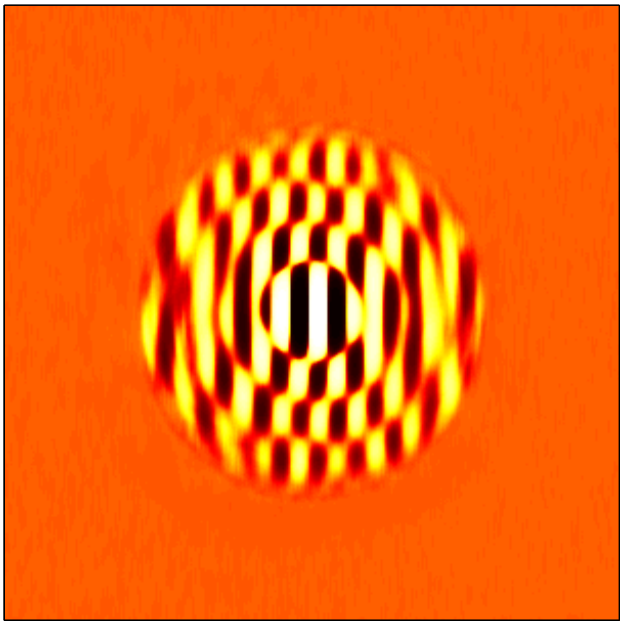

Quantum Optics and Quantum Information group
This project was supervised by:
Drs. H. Di Lorenzo Pires
Dr. M.P. van Exter

Contents

1 Introduction

Though very common in every day life, incoherent light sources are relatively scarce in optics experiments. Most experiments are easier to perform using a coherent light source, but incoherent light sources can hold interesting results of their own. We build a partially coherent light source of which the amount of coherence could be varied. This source was used to perform measurements on some of the properties of the partially coherent light.

One of these properties was the orbital angular momentum spectrum of the light. Previously similar measurements have been performed to obtain the orbital angular momentum distribution of the two-photon field [1]. To the best of our knowledge, this is the first time a partially coherent source is analysed in this way. The results of this experiment have been submitted, the latest version of the submission has been added to this thesis as an appendix.

Using a mostly identical setup we are also able to make a direct visualisation of the coherence function of our source. In this thesis we will describe our method for doing so and study two specific cases, of partially coherent light with zero and non-zero net orbital angular momentum. The latter has been subject of a previous study by another group [2]. We will try to reproduce these results.

2 Theory

In our setup (see section 3.1) we have an incoherent lightsource followed by two circular apertures. The cross-correlation function directly behind the second aperture can be found using the van Cittert-Zernike theorem and [3] is given by

$$W(\boldsymbol{\rho_1}, \boldsymbol{\rho_2}) = T(\rho_1)T(\rho_2)\frac{J_1(\alpha|\boldsymbol{\rho_1} - \boldsymbol{\rho_2}|)}{\alpha|\boldsymbol{\rho_1} - \boldsymbol{\rho_2}|}e^{\frac{i\pi}{\lambda L}(\rho_1^2 - \rho_2^2)} \tag{1}$$

Here $J_1(\rho)$ is the first order Bessel function and $\alpha = \pi d_1/\lambda L$. $T(\rho)$ is the transfer function of the second aperture, a top-hat function. The transverse position $\boldsymbol{\rho_1}$ is a point in the coherence function and $\boldsymbol{\rho_2}$ is that same point translated by the image rotator. Because we rotate around the origin $|\boldsymbol{\rho_1}| = |\boldsymbol{\rho_2}|$, so using the law of cosines we find

$$|\boldsymbol{\rho_1} - \boldsymbol{\rho_2}| = \sqrt{2\rho^2 - 2\rho^2\cos\theta} = 2\rho\sin\left(\frac{\theta}{2}\right) \tag{2}$$

Equation 1 can then be written as

$$W(\rho) = T(\rho)\frac{J_1(f(\theta)\rho)}{f(\theta)\rho} \tag{3}$$

With $f(\theta) = 2\alpha \sin\left(\frac{\theta}{2}\right)$. Thus $f(\theta)$ can be seen as a scaling factor for the Bessel function.

3 Experiment

3.1 Setup

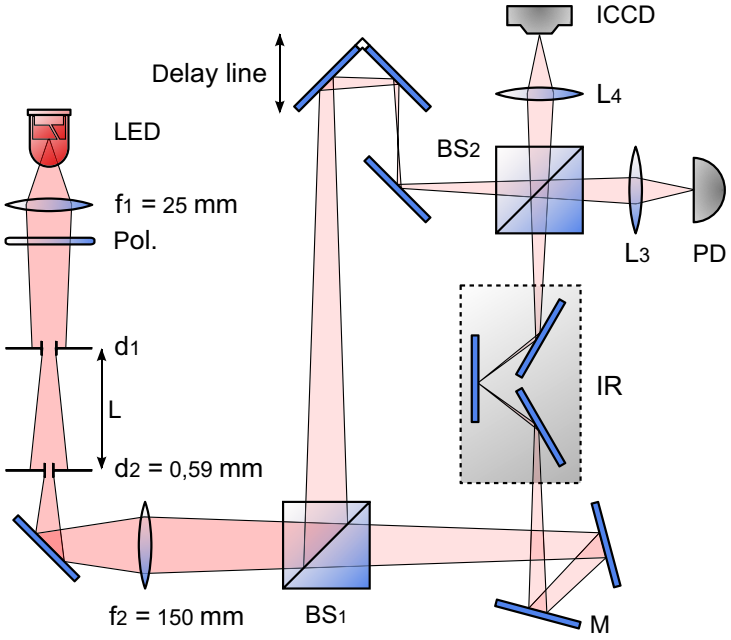

Figure 1: The experimental setup used for the experiment.

Two setups were used. The original setup that we used to get most of our results is depicted in Figure 1. As a light source we used an 826 nm infra-red LED. A lens with 25 mm focal length creates a 15× magnified image of the LED on a circular adjustable aperture. The aperture selects a uniform spot from the LED image. Because light coming from different points of the LED is spatially incoherent, light emitted from the adjustable aperture should be spatially incoherent as well. A second circular aperture with a diameter of 0.59 mm is placed 21 cm after the first. This part of the setup we refer to as the illumination.

By changing the diameter of the first aperture we have control over the coherence of the light from the illumination, that is the amount of spatial modes the light has.

The beam generated in this way is sent through a Mach-Zehnder interferometer. One of the arms of the interferometer contains an image rotator (IR), a device which, as the name implies, rotates an image around its axis. A 150 mm lens creates a $4\times$ magnified image of the second aperture in centre of the image rotator. Because the image rotator hardly changes the polarization upon image rotation, polarization selection is unnecessary. The images from both arms are recombined by BS2 and can be looked at using either a photodiode (PD) or an intensified CCD (ICCD). One of the arms contains a delay line used to make both arms have the same length.

The photodiode measures the total intensity of the transmitted beam. Using a piezo on mirror M the path difference between both arms can be changed slightly within a couple times the wavelength of the light. The resulting intensity changes measured by the photodiode give us the visibility of the interference.

3.1.1 Limitations of the setup

When looking at the intensity of the light emitted from the second aperture as a function of the area of the first aperture, we notice that for small apertures there is a linear relation. The measurements we performed for aperture widths of 1 and 2 mm fell in this regime. However, when the aperture grows beyond 2.5 mm the intensity starts levelling off, making accurate measurements at higher Fresnel numbers impossible. The magnified image of the LED on the adjustable aperture is several times larger than this, so spatially 'more light is available'. The problem then lies in Fourier space, where angles are limited by the opening angle of the light coming from the lens after the LED. Once this maximum angle is reached, opening the first aperture further will not cause any new light to reach the second aperture.

3.1.2 A better illumination scheme

The limitation of the previous setup with regards to higher Fresnel numbers led us to consider another setup. In the previous setup the first aperture is on the near field of the LED. The second aperture is placed 21 cm further in a sort of quasi-far field. In the new setup an additional lens creates a real far field image on the second aperture. Not only does this make the illumination scheme cleaner, but by bundling the light between both apertures we should also be able to reach higher Fresnel numbers.

Unfortunately the scheme failed for practical reasons. The beam emitted from the first aperture became wider than the new lens, effectively turning this lens into a new aperture in a quasi-far field. Thereby this setup inherited

exactly those properties and limitations of the first setup that we had set out to overcome.

3.1.3 Spiral phase plate illumination scheme

Up to this point our illumination setups produced light with a net orbital angular momentum of zero. We have also adopted the setup to make measurements using light with a net orbital angular momentum unequal to zero. In this scheme a spiral phase plate is placed where previously the second aperture was placed, which itself is moved 16 cm further. Two lenses in a f-2f-f configuration create a sharp image of the wave plate on the second aperture. Effectively then, both the spiral wave plate and the second aperture are now in the same plane.

3.2 Experimental Details

3.2.1 Aligning

LED It was important for the experiment to somehow extract from our LED-source a uniform spot of light. To achieve this we produced a magnified image of the LED on an aperture, and cut a uniform part of the image out. The light-emitting part of the infra-red LED has a rectangular shape with a dark spot in the centre and four dark ribs extruding from the centre spot towards the corners. These features made it easy to produce a sharp image of the LED on the aperture. The magnification of the LED needed to be large enough to allow the first aperture at its widest setting needed for the experiment to fit comfortably between two ribs and an edge of the LED image.

A wire crosses over one of the sides of the rectangle to the centre spot. Because this wire is at a different height it might not be directly visible when the rectangle itself is in focus. Nonetheless it is useful to look where the wire is located, and choose a different spot of the LED to place the aperture.

Adjustable aperture The circular adjustable (first) aperture used in the experiment has a scale on it indicating its current diameter. In an effort to find out whether this scale could be trusted we found out that the aperture showed some hysteresis. To measure the real width of the adjustable aperture we made a sharp image with $1\times$ magnification of it on a CCD camera. When the aperture is 'opened up' from one width to another larger width, we found that the scale indicated a value

approximately 0.1 mm higher then the actual width of the aperture. When the aperture was closed from one width to another smaller width, the scale indicated a value approximately 0.2 mm lower then the actual width of the aperture.

In our analysis of the data we had to take this offset into account.

Interferometer The interferometer was aligned using the two beamsplitters. The first beamsplitter was used to align the images from both arms in the near field, the second beamsplitter did the same in the far field.

In those instances where the interferometer was very badly misaligned, it was often useful to remove the rotator from the setup and align the interferometer without it, before putting it back in.

To make the length of both interferometer arms equal we used a LabView program that was already available. Usually it was easiest to first use this program while sending a diode laser through the setup before attempting the LED light which, due to its far shorter coherence length, required finer optimisation.

Rotator To align the image rotator we used the procedure that Bastiaan Florijn described in his bachelor thesis [4]. Changing the alignment of the image rotator had a slight effect on the alignment of the interferometer, so occasionally we had to iterate between the two a couple of times to get them both optimally aligned.

Spiral wave-plate Working on the phase plate illumination scheme described in section 3.1.3 we had to produce a sharp, $1\times$ magnified image of the phase plate on the second aperture using an f-2f-f imaging system. In order to do this we used a special alignment tool. First we aligned the lenses in the directions orthogonal to the beam. Having done that we created a rail on the optics table that confined the lenses to being moved along the beam only.

The alignment tool, a plate containing a series of rectangular holes, was placed at the supposed position of the wave plate. A mirror replaced the second aperture at its exact position, this could be done easily by putting the mirror in the aperture's mount. Light coming through the rectangular holes of the alignment tool were now supposed to go back and forth through the imaging system containing the two lenses and the mirror, and create an image of those rectangular holes on the tool itself. The position of the lenses and tool was optimized to create a

sharp image. The magnification was cbecked by measuring the distances between the optical components.

Then the mirror was replaced with the aperture again, and the alignment tool with spiral phase plate. Once the spiral phase plate was in the exact same place the tool held previously, a sharp image of the wave plate was visible on the aperture. The point of a needle like shape on the image, caused by the phase step in the wave plate, was placed exactly over the aperture. This caused a dark spot to appear in the far field image of the aperture, which in a final round of fine tuning was moved towards the centre of the far field.

3.2.2 Rings

Even though the illumination setup produced a pretty uniform spot of light, the image at the end of the interferometer contained rings. The origin of the rings was tracked down to lens 2 (see Figure 1), spherical aberrations were to blame. We were able to minimize the amount of rings by using a good lens.

4 Measurements and Results

We performed two kinds of measurements by either using either the Photodiode or the ICCD to look at the output of the interferometer (see Figure 1). The photodiode was used for the orbital angular momentum spectrum measurements. The ICCD was used to create pictures of the coherence function of our light source.

4.1 The OAM spectrum

4.1.1 Photodiode measurements

For measurements of the orbital angular momentum spectrum of we used a photodiode. A LabView program was written to make automatic photodiode measurements. The program makes a large number of intensity measurements while slowly moving the piezo mirror. Assuming that the intensity as a function of piezo location is described by a sine, one can obtain the maximum and minimum intensities by putting the measurements in intensity-bins. At the maxima, where the derivative of the sine is lowest, most measurements are made, so the bins with the highest number of measurements correspond to the maximum and minimum intensities. The program then calculates the

visibility using

$$V = \frac{I_{max} - I_{min}}{I_{max} + I_{min}} \tag{4}$$

The LabView program repeats these measurements for a pre-defined series of rotator angles.

The cross-correlation function can be decomposed into modes with a seperated radial and angular part as

$$W(\boldsymbol{\rho_1}, \boldsymbol{\rho_2}) = \sum_l P_l e^{il(\phi_1 - \phi_2)} F_l(\rho_1, \rho_2) \tag{5}$$

Here the radial function $F_l(\rho_1, \rho_2)$ is normalized. By integrating over the radial part and writing $\theta = \phi_1 - \phi_2$ we can obtain a function for the visbility as a function of θ

$$V(\theta) = \sum P_l \cos l\theta \tag{6}$$

So using the visibility curves we can obtain the orbital angular momentum modes (P_l) by Fourier transformation.

4.1.2 Results

We did a number of measurement series to find the visibility as a function of the rotator angle. Figure 2 shows two of these series for two different amounts of coherence. The peaks of these curves have been normalized to 1. By Fourier

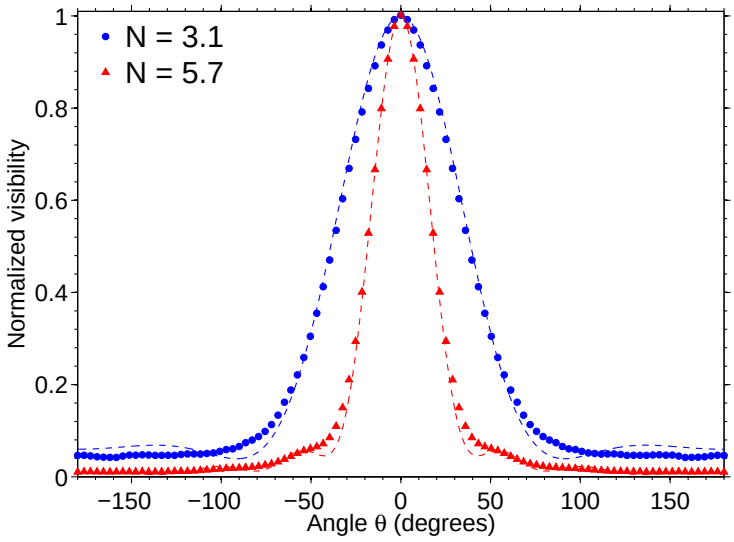

Figure 2: Visibility as a function of angle.

transforming these results we obtain the orbital angular momentum mode distribution, shown in Figure 3. From these figures it is clear that the amount

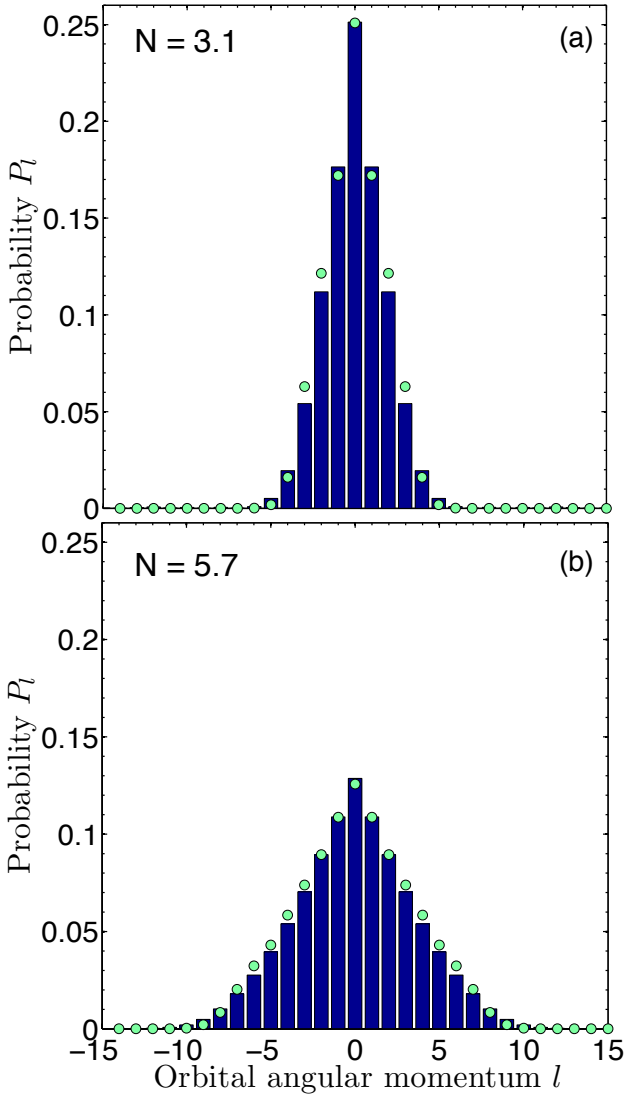

Figure 3: OAM mode distribution.

of modes is higher for a less coherent source. Also there is a clearly defined cutoff point.

4.2 The coherence function

4.2.1 ICCD measurements

When taking an ICCD picture we measure the following intensity

$$I_{tot} = |E_1 + E_2 e^{i\phi}|^2 = I_1 + I_2 + 2Re(\langle E_1^* E_2 \rangle e^{i\phi}) \tag{7}$$

Because we're only interested in the interference term in the above expression, we measure not only I_{tot} but also I_1 and I_2 separately by blocking one arm of the interferometer. Furthermore each intensity is the sum of the light coming from the interferometer, plus some background light and electronic offset of the ICCD. To also get rid of that last term, we perform a measurement with both interferometer arms blocked. To find the 'interference intensity' we then subtract those measurements using

$$I_{intf} = I_{tot} - I_1 - I_2 + I_{block} \tag{8}$$

An additional advantage of this method is that small imperfections of our beam, like for instance the previously mentioned rings, are hardly visible in our final pictures.

By making slight changes to the path difference between both interferometer arms using the piezo mirror we affect the visibility of our interference patterns. We're only interested in pictures where the visibility is at a maximum, this corresponds with specific position of the piezo mirror. Carefully finding those positions for measurements was regretfully impossible due to drift. The path difference was continuously undergoing small changes, so if you would find a maximum, you wouldn't stay there long enough to take a picture. To deal with this problem we changed our strategy by taking a lot of measurements while slowly ramping up the piezo element. Then, we selected the best measurements in the set for analysis. Figure 4 shows the cross sections of the measurements in one of these series.

4.2.2 Results

We produced two kinds of ICCD pictures. For the first we deliberately misaligned the second beamsplitter, with the purpose of creating fringes in our interference pattern. Thanks to these fringes it is easy to spot phase differences. Furthermore intensity minima and maxima are visible regardless of the position of the piezo mirror, so we didn't have to worry about drift. One of these measurements – at the maximum rotation angle (180 degrees), after Equation 8 has been applied, smoothed out and with enhanced contrast to make the fringes better visible – is shown in Figure 5.

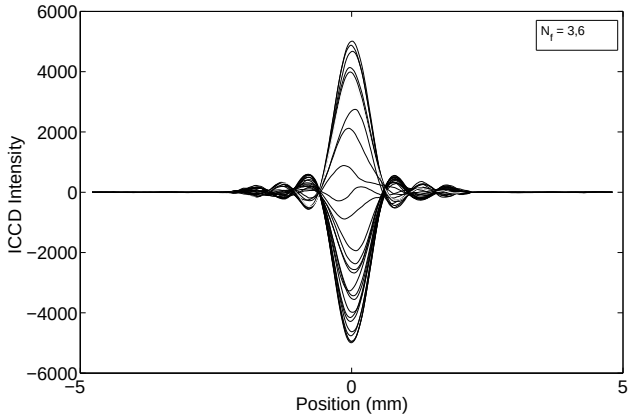

Figure 4: Cross sections of a series of ICCD measurements.

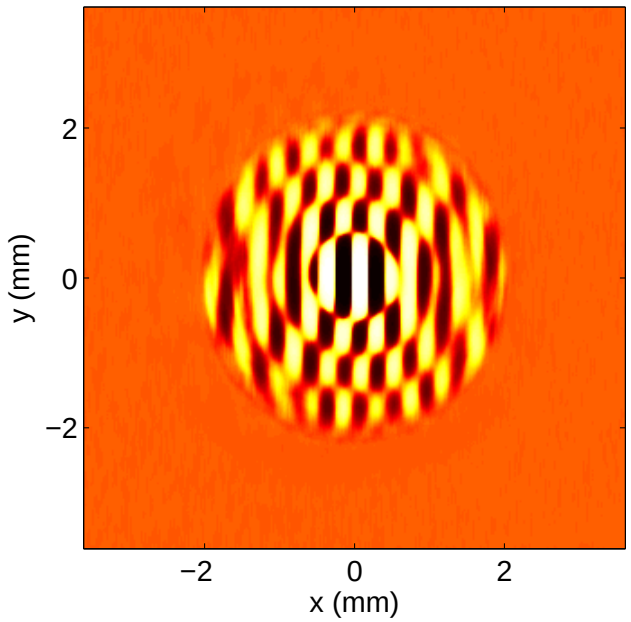

Figure 5: A coherence picture with fringes. The contrast has been enhanced to make the fringes better visible.

For the second kind of pictures the second beamsplitter is properly aligned, so no fringes are visible. In these cases the visibility of the image depends on small path differences between both arms, drift becomes an issue and we need to take several pictures in order to obtain a nice high-visibility one, as described previously. An example of these kind of images, also after Equation 8 has been applied, is shown in Figure 6.

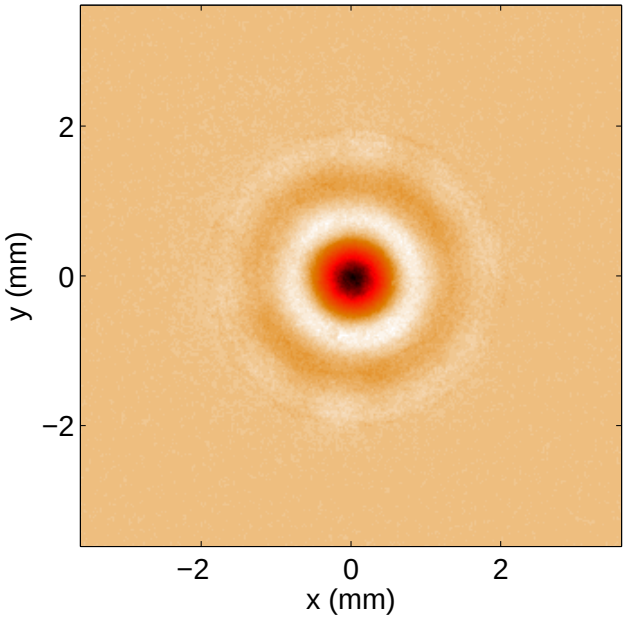

Figure 6: A coherence picture without fringes.

Because of the spherical symmetry of pictures like Figure 6 all the information contained in them can also be displayed in a radial intensity profile. This can be obtained by taking a horizontal cross section of the image or by radial averaging. We wrote a MathLab program to perform radial averaging, but found that the better results were obtained by averaging over a cross-section several pixels wide through the centre of the image. The resulting curves for five different rotation angles is shown in Figure 7. These curves have all been normalized to one.

The scaling effect described by Equation 3 is clearly visible. If we plot the curve predicted by 3 together with one of these measurements, as in Figure 8, we see that theory and experiment are in excellent agreement.

So what does it mean? From Figure 7 we notice that the area of strong coherence reduces from covering the entire spot at a rotation angle of zero degrees to only a small area in the centre at a maximum rotation angle of 180 degrees. This can be made intuitive if one realizes that the cross-correlation function, Equation 1, only depends on the distance between a point and its translated self. When rotated, the further a point is from the centre of the rotation axis, the further it is displaced by the rotation. This translates to a circular area of coherence which becomes smaller as the image rotator is turned further. Points at the centre however are hardly displaced at all, and so rotation leaves the visibility at the centre untouched.

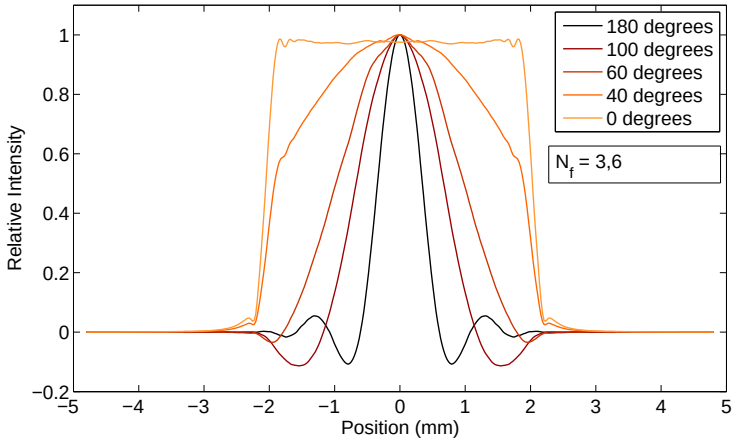

Figure 7: Coherence picture cross sections for different rotation angles.

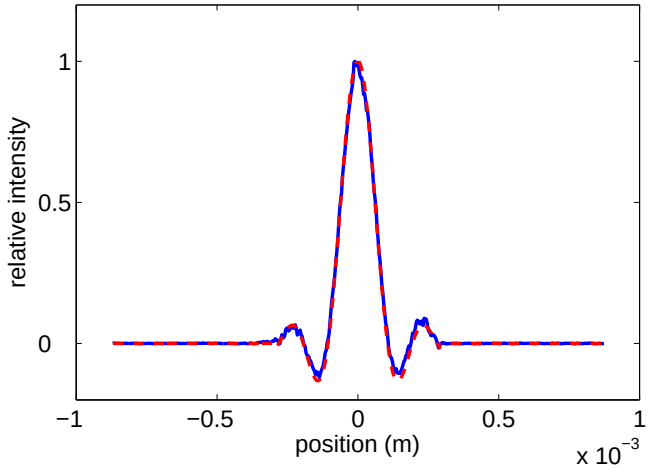

Figure 8: An experimental cross section (blue line) compared with theory (red dotted line).

But Figure 7 also shows us that the coherence away from the centre for a rotated image doesn't go to zero, but alternates between plus and minus. Figure 5 shows that there is a phase jump π between two consecutive coherence areas. For this strange effect I have no intuitive explanation.

4.2.3 Spiral phase plate

Our first measurements using the setup containing the spiral phase plate described in section 3.1.3 wasn't successful. When we compare the results of

these measurements, ICCD pictures of the second aperture far field with a phase plate (Figure 9) and without one (Figure 10), then we notice that the picture without the phase plate does show some weird additional structure in the centre, but it isn't clear whether there is another phase jump there.

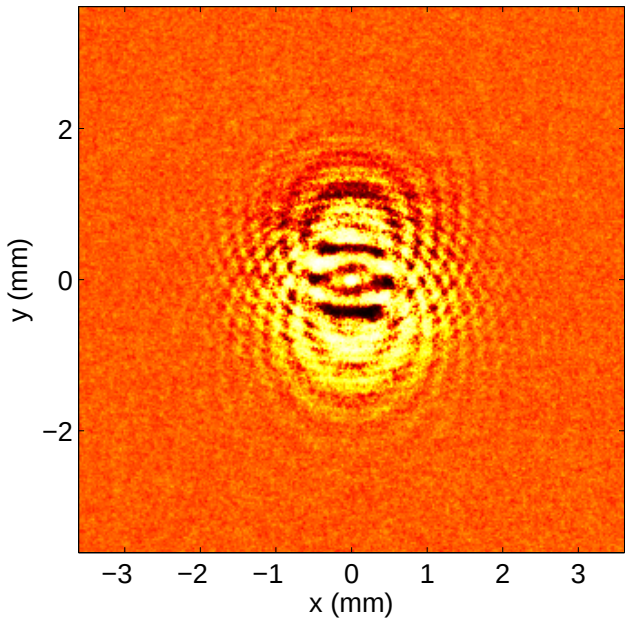

Figure 9: Farfield with phase plate.

After we found these disappointing results we figured out that it is not surprising we didn't produce nice pictures. According to the paper that contained the results we were trying to reproduce [2], the diameter of the new ring we were hoping to see should be only a couple of pixels large in our setup. A number of very recent measurements using a different setup, that most importantly introduces an additional magnification, does show the new phase jump. Figure 11 shows such a measurement.

4.3 Power per mode

During the experiment we have made many minor and larger revisions to our setup. Most of these revisions concerned the illumination scheme in the setup. As a way to test the quality of our variable-coherence source, we occasionally put a photodiode directly behind the second aperture, and measured the total power of the light coming from the aperture as a function of the diameter of the adjustable aperture squared. This is proportional to the aperture's surface, so we expect a linear behaviour.

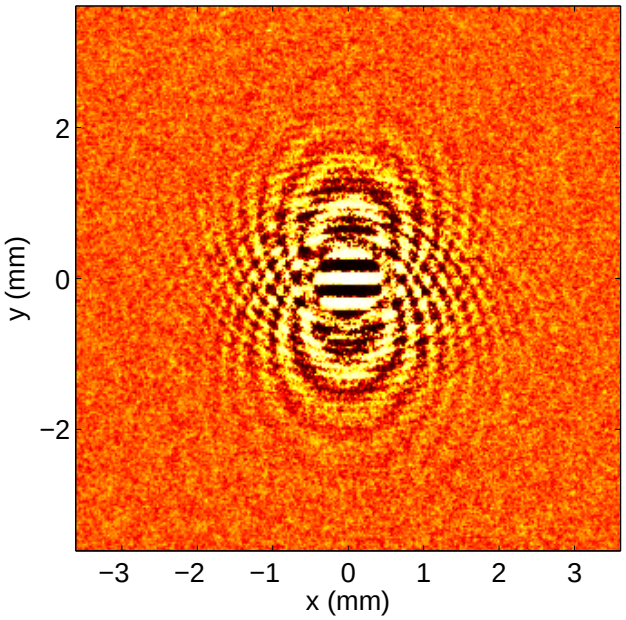

Figure 10: Farfield without phase plate.

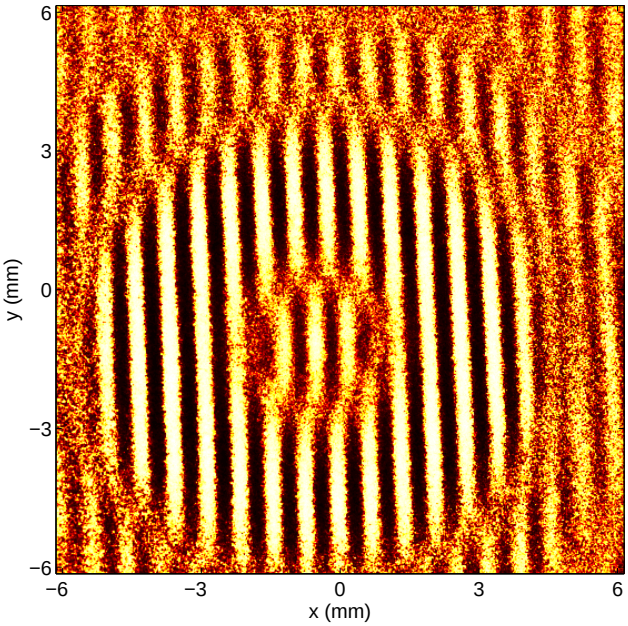

Figure 11: The circular region in the centre, out of phase with the area around it, doesn't show up when the phase plate is removed.

As we desribed in section 3.1.1, this is only part of the story. The LED and the lens placed directly after it emit light in a certain maximum angle, effectively functioning as an additional aperture. When the diameter of the adjustable aperture becomes big enough this maximum angle of our light source starts to play a role, and the power profile levels of. Figure 12 shows two of these power curves for different setups. On the horizontal axis is the two-dimensional Fresnel number, given by

$$N_f^2 = \left(\frac{d_1 d_2}{\lambda L} \right)^2 \tag{9}$$

Where d_1 are d_2 are the diameters of the two apertures, L is the distance between them and λ the wavelength of the light. As can be seen this number is proportional to the surface of the adjustable aperture.

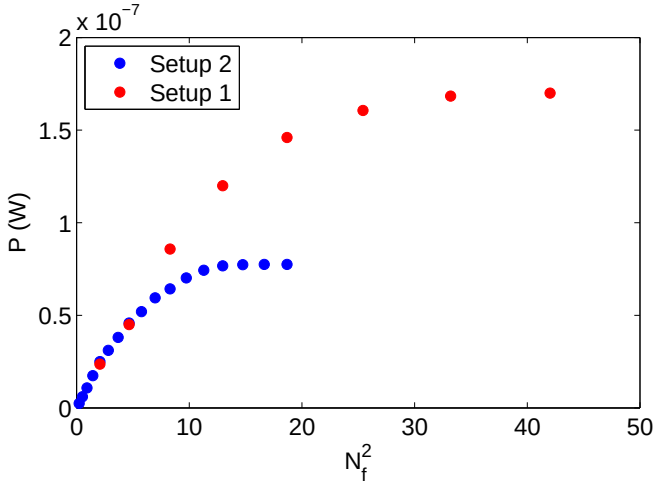

Figure 12: The power per mode. Setup 1 is suitable for measurements at higher Fresnel numbers than setup 2.

It is interesting to note that both power profiles have the same slope before they flatten of. This slope, the power per mode, turns out to be a quality fundamental to the LED source itself and cannot be changed by altering the setup.

5 Discussion

In conclusion, we have built a partially coherent source and used it to obtain the orbital angular momentum spectrum for partially coherent light. The spectrum is in good agreement with our theoretical predictions.

We have also demonstrated a method to directly visualize the coherence function. For partially coherent light with no net orbital angular momentum we again have a good agreement between experiment and theory. For a situation with net angular momentum we have so far managed to replicate the results from a previous paper. As a follow-up experiment it would be interesting to see how the additional coherence region develops when the image rotator is turned.

The hardest part of the experiment was building a good illumination scheme, and this is a place where more improvements can still be made. Our illumination schemes prevented us from performing measurements at Fresnel numbers as high as we'd have liked. Other illumination schemes capable of reaching higher Fresnel numbers can be considered.

A Paper on the measurement of the orbital angular momentum spectrum

The results of the first part of my bachelor project are the subject of a paper written by Henrique Di Lorenzo Pires. The latest version of this paper, that has as of writing not yet been published, is included for your convenience.

References

[1] H. Di Lorenzo Pires, H. C. B. Florijn, M. P. van Exter, Phys. Rev. Lett. **104**, 2 (2010)

[2] D. M. Palacios, I. D. Maleev, A. S. Marathay, G. A. Swartzlander, Phys. Rev. Lett. **92**, 14 (2004)

[3] L. Mandel and E. Wolf, Optical Coherence and Quantum Optics, ISBN 0-512-41711-2

[4] H. C. B. Florijn, Interference of two high dimensional entangled photons